Sensors and Materials, Vol. 13, No. 8 (2001) 433–443
MYU Tokyo

S & M 0460

Near-field Scanning Optical Microscope Based on Fast Birefringence Measurement

Shinya Ohkubo and Norihiro Umeda

Faculty of Technology, Tokyo University of Agriculture and Technology
2-24-16, Nakacho, Koganei, Tokyo 184-8588, Japan

(Received April 6, 2001; accepted September 5, 2001)

Key words: birefringence, near-field optics, microscope, scanning, polarization, fiber probe

A new optical configuration for a near-field scanning optical microscope with birefringence contrast imaging is described. A fast and accurate birefringence measurement system has been installed into an illumination mode near-field microscope. Birefringence is measured by using left and right hand circularly polarized laser beams with different frequencies, which are generated by an axial Zeeman laser. A sample is illuminated by the light of two circularly polarized components through a fiber probe tip. The measurement characteristic of the developed system and images of birefringence material are shown.

1. Introduction

The advent of near-field scanning optical microscopy (NSOM) allows for the development of instruments with a resolution beyond the diffraction limit.[1] In the early study of near-field optics, localized light intensity near a sample surface was used as a detection quantity in most developed near-field optical microscopes.[2] According to further developments in near-field optics, various NSOM instruments that can detect an optical phase or spectroscopic quantity have been developed. Some polarization contrast NSOMs have been proposed, since polarization is necessary for measuring the orientation of polymer materials and the phase transition of liquid crystals, cell structure analysis, and stress analysis of solid materials . Betzig and Tautman, who first realized a polarization contrast NSOM with cross Nicol prisms,[3] obtained a near-field image for magneto-optic recording bits.[4] However, a quantitative analysis of the polarization property in a sample is difficult; therefore, novel polarization NSOMs that are able to measure dichroism and birefringence have been discussed and studied. Although Vaez-Iravani and Toldo-Crow developed the polarization NSOM using an electro-optic phase modulator,[5] the azimuth angle of bire-

fringence cannot be measured. On the other hand, a polarization modulation NSOM which allows for simultaneous imaging of both the magnitude and direction of optical anisotropy was investigated,[6] and the imaging of a dichroic single crystal of rohdamine 110 was demonstrated. Optical anisotropy, in particular, the birefringence contrast of NSOM, has received a great deal of attention in many fields, for example, optical memory, biology, polymers and liquid crystals.

It is necessary to adopt a fundamental birefringence measurement method in order to realize a birefringence contrast NSOM. To date, various birefringence measurement methods have been developed. For example, although a heterodyne interference technique has a high measurement accuracy,[7] the measurement takes a long time. In the NSOM, a measurement time of approximately 100 microseconds is desired for each sampling point in order to scan a probe on a sample surface. Therefore, in our study, a fast birefringence measurement method is developed, and the measurement performance is clarified in order to apply it to the NSOM.

In this paper, the principle of the fast birefringence measurement and its performance are described in Sec. 2, and a system configuration of a birefringence NSOM and images of birefringence samples are shown in Secs. 3 and 4, respectively. Finally, the conclusion is given in Sec. 5.

2. Fast Birefringence Measurement

2.1 *Principle*

Figure 1 shows the birefringence measurement system.[8] A frequency stabilized axial

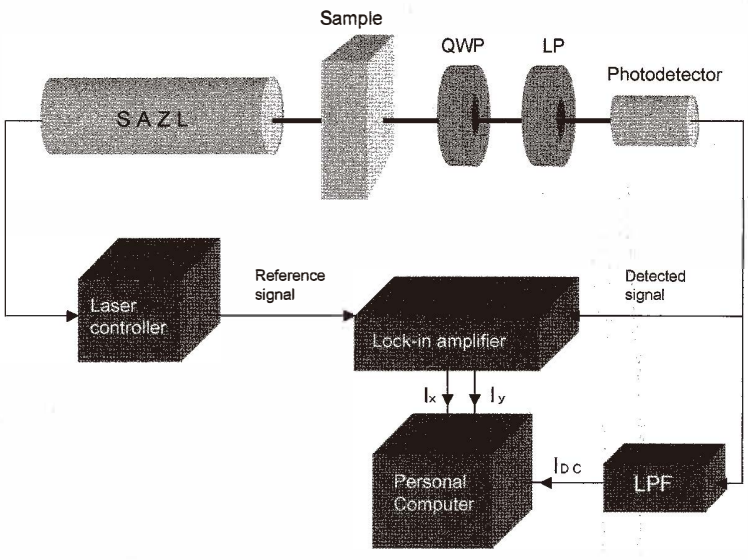

Fig. 1. Schematic diagram of birefringence measurement system.

Zeeman He-Ne laser in an axial magnetic field (SAZL) oscillates two components which consist of right and left circularly polarized lights with a difference in frequency of 70 kHz. Passing through a sample to be measured, the laser beam goes to a quarter-wave plate (QWP) with a fast axis of 45 deg, and a linear polarizer (LP) with its transmission axis parallel to the horizontal plane. The emergent beam from the LP is incident onto a photodetector. The output signal from the photodetector consists of AC components and a DC component. The former is generated by mixing two components of the axial Zeeman laser to obtain a beat signal.

The optical system shown in Fig. 1 can be represented by the Stokes vector and Mueller matrices as follows,

$$\boldsymbol{S} = \mathrm{L} \cdot \mathrm{Q} \cdot \mathrm{X} \cdot \boldsymbol{S}_{ax}, \tag{1}$$

where L, Q and X are the Mueller matrices of the linear polarizer, quater-wave plate and sample, respectively, and $\boldsymbol{S}$ and $\boldsymbol{S}_{ax}$ correspond to the Stokes vector of the emergent beam and that of the axial Zeeman laser beam. For simplicity, we use an approximation of measured retardation that is smaller than unity. As a result the detected component which is proportional to the intensity component of the Stokes vector is given by

$$I = \frac{a_r^2 + a_l^2}{2} + a_r a_l \sin\Delta\cos 2\phi \cos\omega_b t + a_r a_l \sin\Delta \sin 2\phi \sin\omega_b t, \tag{2}$$

where a_l and a_r are amplitudes of the left- and right-hand circularly polarized components, ω is the angular Zeeman difference frequency between the two components, and Δ and ϕ are the retardation and azimuth angle of a sample, respectively. From eq. (2), the DC component I_{dc} and quadrature AC components of beat signals I_x and I_y are given by

$$I_{dc} = \frac{a_r^2 + a_l^2}{2}, \tag{3}$$

$$I_x = a_r a_l \sin\Delta\cos 2\phi, \tag{4}$$

$$I_y = a_r a_l \sin\Delta\sin 2\phi. \tag{5}$$

In eqs. (3), (4) and (5), since we can adjust the amplitudes of the left and right circular polarization components to be equal; *i.e.*, $a_l = a_r$, the retardation Δ and the azimuth angle of the fast axis ϕ of the sample are calculated as follows,

$$\Delta = \sin^{-1}\left\{\frac{\sqrt{I_x^2 + I_y^2}}{I_{dc}}\right\}, \tag{6}$$

$$\phi = \frac{1}{2}\tan^{-1}\left\{\frac{I_y}{I_x}\right\}. \tag{7}$$

In Fig. 1, I_{dc} is filtered from the detected signal by using a low-pass filter (LPF) with a cut-off frequency of 100 Hz, and I_x and I_y are synchronously detected by a two-phase lock-in amplifier. A controlling beat signal from the SAZL is used as a reference signal of the lock-in amplifier. I_{dc}, I_x and I_y are converted to digital data by means of an analog to digital converter, and sent to a personal computer (PC) in order to calculate Δ and ϕ by using eqs. (6) and (7).

2.2 *Measurement performance*

In general, a fast imaging speed of NSOM is desirable for avoiding thermal drift of the translation scanner, and for observing a fluid biological sample. It is also desirable in the birefringence contrast NSOM. Therefore, it is necessary to shorten the measurement time of birefringence. For example, in the case of an imaging time of 2 s for a 128 × 128 pixel, the required measurement time for birefringence taken per pixel must be less than 100 μs.

In order to evaluate the measuring time of the method, we measured a standard deviation for the fixed birefringence of Babinet-Soleil compensator data as a function of a time constant of the lock-in amplifier (LIA) and the acquisition interval time to the PC. The standard deviations of 100 measuring data were calculated for the constant acquisition time of 1 msec and for the time constant of 100 μs. The results are shown in Figs. 2 (a) and (b), respectively. From these figures, both the minimum time constant of the LIA and the acquisition time for realizing a stable and accurate measurement are found to be 100 μsec. Therefore, it is found that the proposed method has satisfactory measurement time for application to the NSOM.

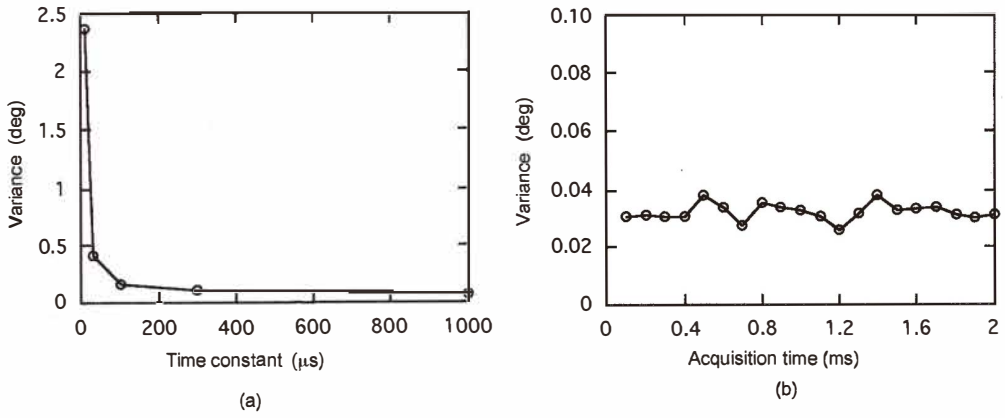

Fig. 2. Experimental results of variance in measured data as a function of time constant of lock-in amplifier (a) and acquisition time to personal computer (b).

If the sample is removed from the experimental setup, we can measure the minimum detectable value which is determined by the instrument noise; principally, shot noise in the photocurrent and electrical noise. The measurement result shown in Fig. 3 for the continuous measuring data gives a minimum detectable retardation of 0.072 deg on average.

3. Birefringence NSOM

3.1 *System configuration*

The birefringence contrast NSOM (B-NSOM) based on the above fast birefringence measurement method was constructed with a shear force regulating technique, as shown in Fig. 4. The light from the SAZL is launched into a single mode optical fiber with an in-line polarization compensator which consists of three fiber loops. This is utilized to compensate for a polarization state change due to stress-induced birefringence in the fiber. The other end of the fiber is pulled to form a tip by means of a melting and pulling method. The emergent light from the fiber tip is recovered into right- and left-hand circular polarizations by the in-line polarization compensator. The typical output intensity from the fiber probe is 0.1 μW for the incident power of 0.75 mW. The light transmitted through a sample goes to an objective (NA = 0.4), a quarter wave plate (QWP45) and a linear polarizer (LP0), and is incident on a photomultiplier (PM). The detected beat signal from the PM is synchronously rectified by a two-phase lock-in amplifier (LIA1) with the beat frequency from the SAZL as a reference signal. The quadrature signals from LIA1 and the dc component of the detected signal are sent to a PC, and the retardation and azimuth angle of the birefringence are calculated by eqs. (6) and (7). The gap between the tip and sample is regulated by a shear force technique, which is commonly used in conventional NSOMs.[9]

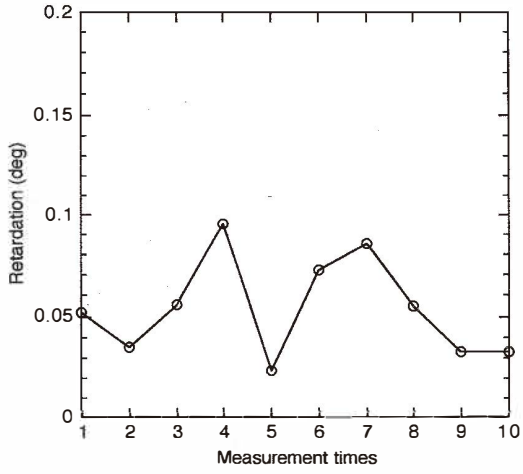

Fig. 3. Minimum detectable retardation without sample.

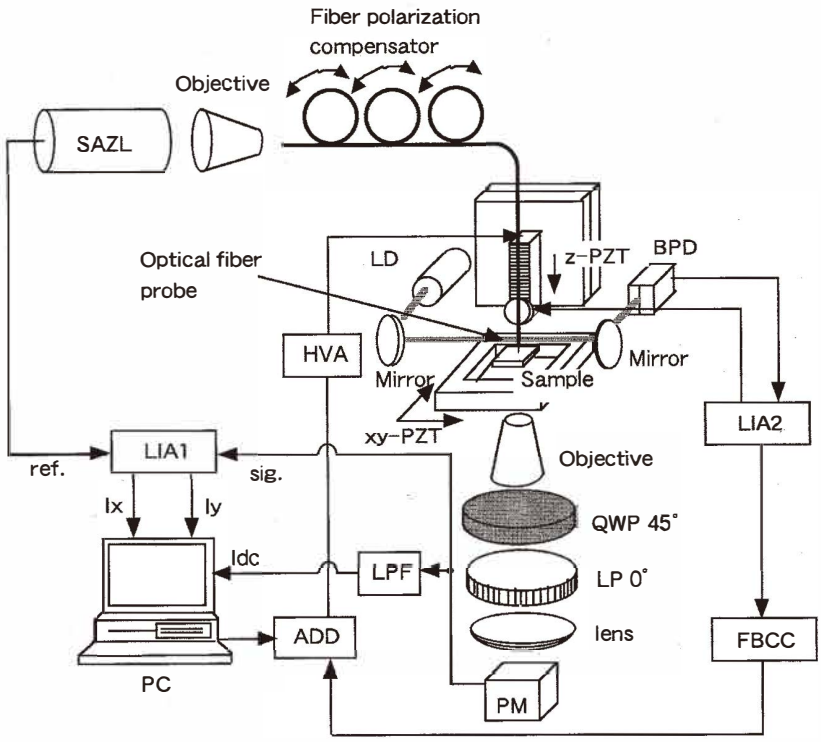

Fig. 4. Diagram of the B-NSOM using right- and left- hand circularly polarized laser.

3.2 *System performance*

(a) Polarization property

The polarization property of emerging light from the gold-film-coated optical fiber probe tip was examined. If the polarization state of the SAZL is maintained to the end of the fiber, the right- and left-hand circular polarization states of the SAZL are converted to orthogonal linear polarization states through a quarter wave plate at an azimuth of 45 deg. Therefore, the minima of the beat signal intensity should appear at four points, when the LP is rotated by 360 deg. The beat signal amplitude of the SAZL was measured when the emerging light from the fiber probe was analyzed by a quarter wave plate and linear polarizer. The measurement result is shown in Fig. 5. The four minima of the beat signal intensity appeared with the LP rotation, though the LP rotation was limited to within 330 deg due to the configuration of the equipment. From this figure, it is confirmed that the lights from the sharpened optical fiber probe preserve the polarization states of the SAZL.

(b) Measurement accuracy

The measurement result when the retardation of the Babinet-Soleil compensator (BSC) changes at a constant azimuth angle to the fast axis is shown in Fig. 6 (a). The straight line

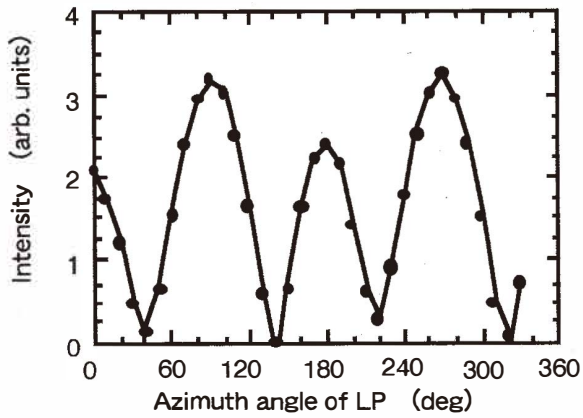

Fig. 5. Measurement result of polarization property for beam emerging from sharpened fiber probe.

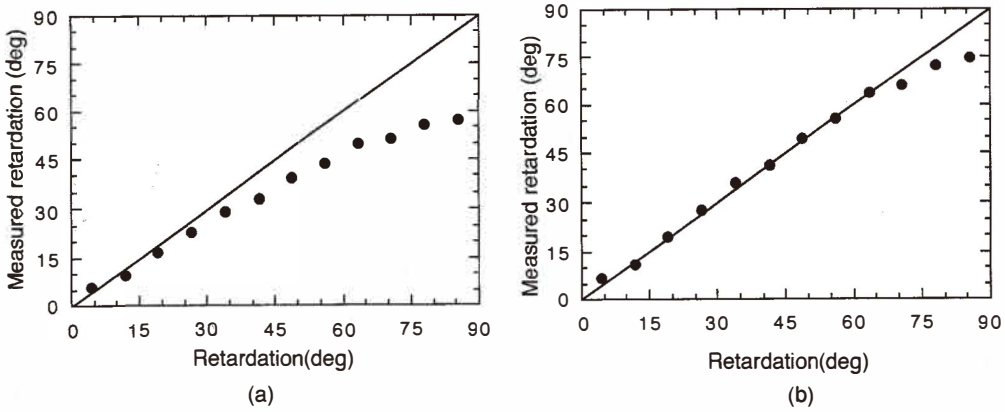

Fig. 6. Measured retardation response upon changing the settings of the Babinet-Soleil compensator (a) before correction and (b) after correction with calibration line.

in the figure is the calibrating line of the BSC. From this, it is found that the measured value differs from the calibrating line of the BSC by more than approximately 30 deg. As the cause of this, the following is considered: the effect of birefringence in the optical fiber is not perfectly cancelled by the in-line compensator and the intensities of the right- and left-hand circularly polarized lights of the SAZL are not equal. Therefore, the measured value was corrected using a correction function obtained from both the calibrating line of the BSC and the measured data shown in Fig. 6 (a). The result after correction is shown in Fig. 6 (b). From this figure, the retardation agrees well with the calibrating line, to within about 60 deg.

The azimuth angle of the birefringence was also measured by the rotation of the fast axis of the BSC at the fixed retardation. The result is shown in Fig. 7. The straight line in

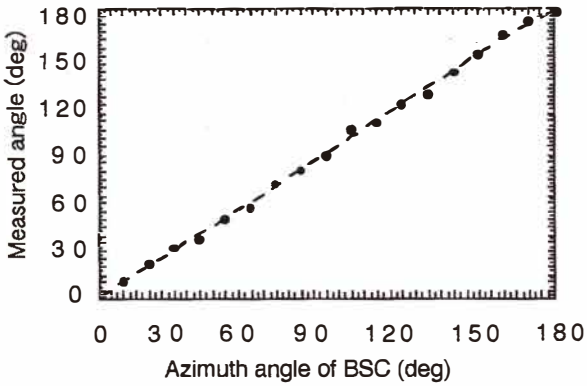

Fig. 7. Measured azimuth angle of birefringence upon changing the azimuth of the Babinet-Soleil compensator.

the figure is the calibrating line of the BSC. There exists an error of 0.4 deg on average and 3.04 deg at maximum, in the measurement of the azimuth angle of birefringence by this method.

4. Observation of Samples

4.1 *Highly oriented polymer film*

We have prepared a highly oriented sample to evaluate the imaging capability of the B-NSOM. The sample was fabricated by a friction transfer technique, wherein the surface of a polymer rod is slid on a clean glass plate.[10] The polymer rod (ethylene vinylacetate) was brought into contact with a heated cover glass slip at 180°C, and was moved by hand at a constant rate and in one direction.

A topographic image of the polymer film fabricated by the friction transfer is shown in Fig. 8 (a). Many corrugation structures with a height difference ranging from 50 to 100 nm can be seen. Figures 8 (b) and (c) are images for the retardation and the azimuth angle of birefringence in the sample. The sliding direction of the polymer rod is parallel to the vertical direction in these figures. Figure 8 (b) shows an inhomogeneous structure in the retardation of birefringence, which appears as bright and dark portions in the vertical direction. This structure is most likely due to the different degree of orientation in the polymer sample. Since the birefringence is proportional to the product of optical phase difference and thickness of the sample, the retardation image in Fig. 8 (b) is mainly influenced by both phase difference and substrate thickness, that is, topography of the sample. However, as Fig. 8 (b) is different from the topography, the retardation image might show an inherent phase difference in the sample.

On the other hand, Fig. 8 (c) shows the mapping of the azimuth angle of birefringence in the sample. In this figure, the direction of each small bar represents the azimuth angle of birefringence at each pixel. The direction bars at each pixel are almost parallel to the sliding direction of the polymer rod during sample formation. The partial disturbance of

the azimuth angle in Fig. 8 (c) might be due to a measurement error caused by small retardation or scattered light from the surface roughness of the sample.

4.2 *Preformat pits of MO disk*

Magneto-optical (MO) disks, which are widely used as a removable/rewritable high-density data storage medium, are produced by an injection molding method with a polycarbonate resin. Preformat pits and grooves are formed by a transcription of a stamper on the surface of the MO disk. Therefore, the surface condition of the disk influences MO data reading. Recently, Umezawa *et. al.* reported characteristic fluctuations in the MO signals around the boundaries between preformat pits and grooves in adjacent bands.[11] It is deduced that such fluctuations may be caused by birefringence around preformat pits.

We investigated a localized birefringence in an MO disk using the developed B-NSOM. Figure 9 shows a schematic diagram of the surface structure of a 3.5 inch 640 MB MO disk with preformat pits. The relative alignment of the preformat pit area shifts between adjacent bands as one moves towards the circumference. The grooves in the

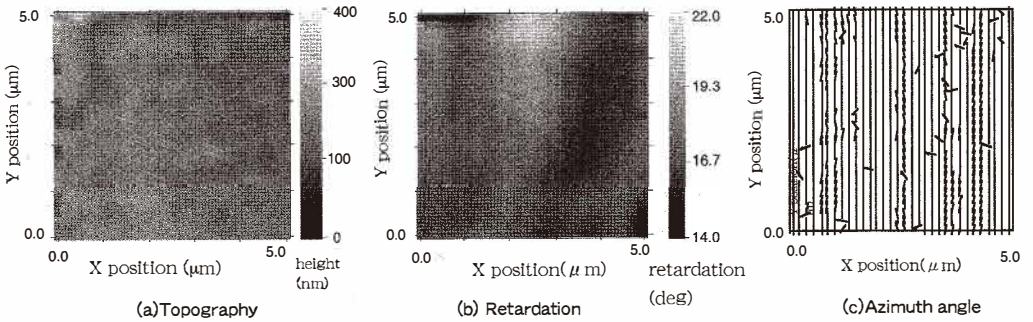

Fig. 8 (a). Topographic image of polymer film. (b) Retardation and (c) azimuth angle of birefringence images of polymer film.

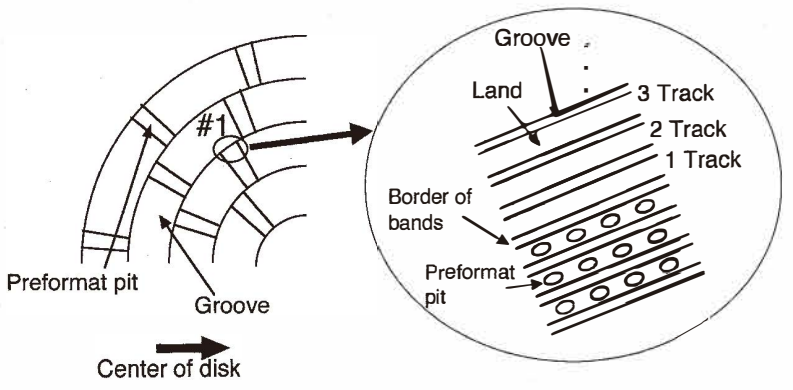

Fig. 9. Surface structure of MO disk.

vicinity of the band border have portions of adjacent preformat pits in the next band. We observed recording tracks around the boundaries between preformat pits and grooves in the adjacent bands (#1) having the previously reported characteristic fluctuations in MO signals.[11] Figure 10 shows a transparent retardation image around the border of a band (preformat pit area called VFO1) in the polycarbonate plastic bare substrate without a magneto-optical thin film. From this image, we confirm that preformat pits exist adjacent to the grooves shown in Fig. 9. Contrast in the retardation image occurs due to both the birefringence of the material itself and a change of a structural feature on the disk surface. It is shown that bright portions in the preformat pit area contain more stress than other portions in the groove area due to the transcription process using a stamper. Therefore, a local stress at the border of bands induces birefringence due to a photoelastical property.

Furthermore, we observed the azimuth angle of birefringence at the horizontal groove shown in Fig. 11. Figure 11 (a) shows a variation of the azimuth angle. As there is no periodical change, the azimuth angle is almost constant in the imaged region. On the other hand, the azimuth angle at the border of the bands is shown in Fig. 11 (b). The figure shows that there is a periodic change of the azimuth angle in which the period corresponds to the interval of the preformat pits. Therefore, the localized periodic change of the azimuth angle may have caused the characteristic fluctuation in the MO signal.

5. Conclusion

We have constructed a new polarization contrast NSOM capable of obtaining the retardation and the azimuth angle mappings of birefringence in a sample. Highly oriented polymer film fabricated by the friction transfer technique was imaged in order to demonstrate the utility of this technique. Also, the birefringence distribution of an MO disk was imaged. As a result, a remarkable variation in the azimuth angle which appears to reflect fluctuation in the MO signal was found. The B-NSOM reported here will be valuable for the evaluation of anisotropic microcrystalline samples and microstress in materials.

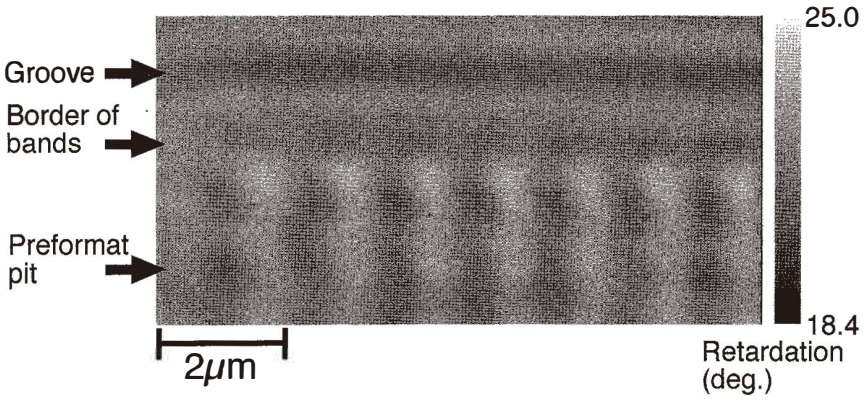

Fig. 10. Retardation image around border of band.

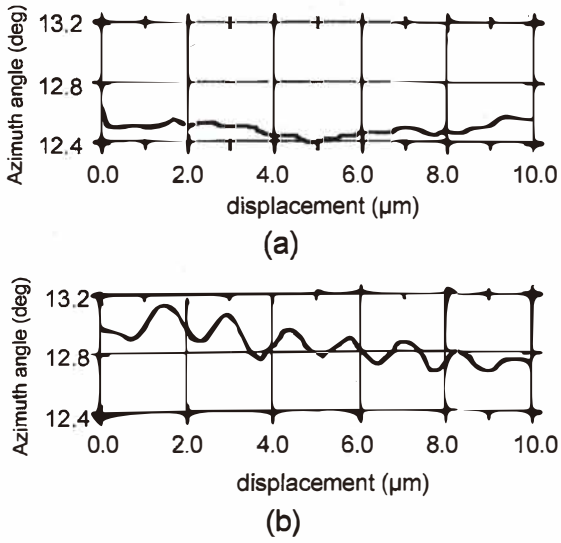

Fig. 11. Variations of azimuth angle at the groove (a) and at the border of band (b).

Acknowledgements

This research was partially supported by a grant-in-aid for scientific research on priority areas #745 from the Ministry of Education, Culture, Sports, Science, and Technology, Japan, and the Takahasi Industrial and Economic Research Foundation.

References

1 E. Betzig and J. K. Tautman: Science **257** (1992) 189.
2 D. Courjon, K. Sarayeddinea and M. Spajer: Opt. Commun. **71** (1990) 23.
3 E. Betzig, J. K. Tratman, L. S. Weiner, T. D. Harris and R. Wolfe: Appl. Opt. **31** (1992) 4563.
4 E. Betzig, J. K.Tautman, R. Wolfe, E. M. Gyorgy, P. L. Finn, M. H. Kryder and C-H. Chang: Appl. Phys. Lett. **61** (1992) 142.
5 M.Vaez-Iravani and R. Toledo-Crow: Appl. Phys. Lett. **62** (1993) 138.
6 D. A. Higgins, D. A. Vanden Bout, J. Kerimo and P. F. Barbara: J. Phys. Chem. **100** (1996) 13794.
7 N. Umeda and H. Kohwa: Electronics and Communications in Japan, Part 2. **74** (1991) 21.
8 N. Umeda, S. Wakayama, S. Arakawa, A. Takayanagi and H. Kohwa: Proc. of SPIE **2873** (1996) p. 119.
9 E. Betzig, P. L. Finn and J. S. Weiner: Appl. Phys. Lett. **60** (1992) 2484.
10 J. C. Wittmann and P. Smith: Nature **352** (1991) 414.
11 T. Umezawa, T. Horiguchi, T. Tomie and K. Nakatani: Jpn. J. Appl. Phys. **39** (2000) 2624.